The Astrophysical Journal, 804:86 (10pp), 2015 May 10 doi:10.1088/0004-637X/804/2/86

A STACKED ANALYSIS OF 115 PULSARS OBSERVED BY THE *FERMI* LAT

A. McCann
Kavli Institute for Cosmological Physics, University of Chicago 933 East 56th Street, Chicago, IL 60637, USA; mccann@kicp.uchicago.edu
Received 2014 December 7; accepted 2015 February 18; published 2015 May 5

ABSTRACT

Due to the low gamma-ray fluxes from pulsars above 50 GeV and the small collecting area of space-based telescopes, the gamma-ray emission discovered by the *Fermi* Large Area Telescope (LAT) in ∼150 pulsars is largely unexplored at these energies. In this regime, the uncertainties on the spectral data points and/or the constraints from upper limits are not sufficient to provide robust tests of competing emission models in individual pulsars. The discovery of power-law-type emission from the Crab pulsar at energies exceeding 100 GeV provides a compelling justification for exploration of other pulsars at these energies. We applied the method of aperture photometry to measure pulsar emission spectra from *Fermi*-LAT data and present a stacked analysis of 115 pulsars selected from the Second *Fermi*-LAT catalog of gamma-ray pulsars. This analysis, which uses an average of ∼4.2 yr of data per pulsar, aggregates low-level emission which cannot be resolved in individual objects but can be detected in an ensemble. We find no significant stacked excess at energies above 50 GeV. An upper limit of 30% of the Crab pulsar level is found for the average flux from 115 pulsars in the 100–177 GeV energy range at the 95% confidence level. Stacked searches exclusive to the young pulsar sample, the millisecond pulsar sample, and several other promising sub-samples also return no significant excesses above 50 GeV.

Key words: gamma rays: general – gamma rays: stars – pulsars: general

1. INTRODUCTION

The Large Area Telescope (LAT) on board NASA's *Fermi* satellite has detected over 150 new gamma-ray pulsars.[1] One seemingly unifying feature seen in all of these pulsars is the form of their spectral energy distribution (SED), which is typically described by a power law followed by a spectral cut-off occurring between 1 and 10 GeV (Abdo et al. 2013). The relatively narrow range of the measured cut-off energy observed in pulsars across a wide range of spin parameters suggests the gamma-ray emission mechanism is common across these pulsars and that it is not strongly dependent on the pulsar spin or energetics. Above the GeV break energy, pulsar SEDs appear to fall exponentially, although for bright gamma-ray pulsars with high statistics above the break, sub-exponential cut offs are preferred (Abdo et al. 2013). Curvature radiation occurring at the radiation-reaction limit in the outer magnetosphere can largely explain these spectral features and thus, models based on this mechanism have become the most favored explanations of pulsar emission in the *Fermi*-LAT era.

From a modeling perspective, the maximum energy of the observed radiation provides robust and model-independent constraints on the altitude of the emission sites above the neutron star (Story & Baring 2014). The shape of the SED above the break is also a key probe of the emission mechanisms, with exponential cut offs predicted in curvature emission models (e.g., Harding et al. 2008) and power-law extensions predicted in inverse-Compton scattering models (e.g., Lyutikov et al. 2012). While curvature emission is broadly accepted as the dominant emission mechanism, many authors, such as Cheng et al. (1986), Romani (1996), Hirotani (2001), and Takata & Chang (2007) have discussed the role of inverse-Compton emission processes in pulsar magnetospheres. The discovery of >100 GeV emission from the Crab pulsar (Aliu et al. 2011; Aleksić et al. 2011, 2012), which strongly disfavors curvature-emission-based models, has led to renewed interest in inverse-Compton studies and Du et al. (2012), Lyutikov (2013), and others, have presented magnetospheric inverse-Compton models that explain emission above the GeV break measured by *Fermi*-LAT. Others, such as Aharonian et al. (2012) and Pétri (2012), have presented inverse-Compton models where pulsed emission at sub-TeV energies originates from acceleration zones outside the light cylinder.

The Crab pulsar is the only pulsar known which clearly exhibits non-exponentially suppressed emission above the GeV break, with power-law-type emission seen to extend to 400 GeV.[2] Studies of the Geminga pulsar show that the SED above the GeV break is compatible with a steep power law (Lyutikov 2012; Aliu et al. 2015), but no emission has been seen above 100 GeV. Recent studies of the Vela pulsar with *Fermi*-LAT data have reported significant emission above 50 GeV (Leung et al. 2014), but again, no significant emission above 100 GeV has been observed. Aliu et al. (2015) argue that even in the case of these two bright pulsars—the brightest known to exist—the available spectral data are not sufficient to discriminate between exponential and power-law-shaped spectra above ∼10 GeV. The *Fermi*-LAT catalog of sources above 10 GeV (1FHL) reports the detection of significant pulsations from 13 pulsars at energies which exceed 25 GeV (Ackermann et al. 2013b). These 13 pulsars are largely drawn from the brightest pulsars observed by the *Fermi*-LAT ($F_{>100\,\mathrm{MeV}} > 1.6 \times 10^{-7}\,\mathrm{s}^{-1}\,\mathrm{cm}^{-2}$) and thus are sufficiently bright to be detected by *Fermi*-LAT at these energies, even as their spectrum falls rapidly above the break. In the second *Fermi*-LAT catalog of gamma-ray pulsars, only four pulsars have a measured flux point above 30 GeV (Abdo et al. 2013) and the statistical uncertainties on the spectral points are too large to provide robust tests of model predictions at these

[1] https://confluence.slac.stanford.edu/display/GLAMCOG/Public+List+of+LAT-Detected+Gamma-Ray+Pulsars

[2] Recently the MAGIC collaboration has presented evidence indicating that the power-law spectrum of the Crab pulsar may extend to TeV energies. See http://fermi.gsfc.nasa.gov/science/mtgs/symposia/2014/abstracts/185.

energies. The question of whether the Crab pulsar is unique, or whether non-exponentially suppressed gamma-ray spectra are common in gamma-ray pulsars is of great importance. Beyond pulsar emission modeling, questions concerning the emission properties of pulsars have significant implications for galactic dark matter searches, where unassociated gamma-ray excesses can be interpreted as the remnants of dark matter annihilation (e.g., Abazajian & Kaplinghat 2012). Since pulsars are likely the main background for these searches, categorizing the shape of pulsar spectra is a critical step toward validating any indirect dark matter signal in the gamma-ray domain. To address these questions, we present a stacked analysis of gamma-ray pulsars to search for non-exponentially suppressed emission above 50 GeV which cannot be resolved in the *Fermi*-LAT analysis of a single object, but can be detected from an ensemble.

The remainder of this paper is structured in the following way. In Section 2 we describe the *Fermi*-LAT data used in this analysis. Section 3 introduces the aperture photometry (AP) method for measuring pulsar spectra and presents an assessment of its performance. In Section 4 we present the results of the stacking analysis and in Section 5 we provide some discussion and concluding remarks.

2. THE PULSAR DATA SAMPLE

This work is based on the 117 pulsars described in the Second *Fermi*-LAT catalog of gamma-ray pulsars (Abdo et al. 2013), which shall be referred to as 2PC throughout. 2PC provides a wealth of measured spectral and temporal characteristics which enable this study. Of particular importance to this analysis is the *Off* peak phase range, which is derived from a Bayesian Block analysis of the pulsar light curve (Jackson et al. 2005; Scargle et al. 2013). This is the interval of the pulsar rotation phase where the pulsed emission is deemed to be at its lowest flux. No *Off* range was defined in the 2PC for PSRJ 2215+5135, thus this pulsar was excluded from the study. Further, while used as the prototype for the analysis methodology, the Crab pulsar was also excluded from this study, since we are investigating whether Crab-pulsar-like emission above ~50 GeV is seen in other pulsars. The exclusion of these two sources reduces the number of pulsars analyzed in this work to 115, a total which comprises 76 young (non-recycled) pulsars and 39 millisecond pulsars.

Beyond the number of pulsars analyzed, the size of the data set used for a given pulsar analysis is entirely dependent on the availability of pulsar timing solutions. Timing solutions encode the spin-down behavior of the pulsar and enable the conversion of the measured photon arrival time to the pulsar rotation phase value. Pulsar timing solutions with periods of validity ranging from 1.4 to 3.3 yr were provided in the supplementary material of the 2PC. For 66 pulsars, updated timing solutions provided by Matthew Kerr[3] (M. Kerr et al. 2014, in preparation) that have periods of validity lasting ~5 yr were chosen over the shorter 2PC timing solutions. Combining the two cases, the average data set analyzed spans 4.2 yr (see Figure 1). It should be noted, however, that longer timing solutions were more often provided for brighter pulsars.

The *Fermi*-LAT pulsar analysis presented here uses Pass-7 reprocessed `Source`-class photon data retrieved from the *Fermi* science support center weekly data server. Data processing was performed using the *Fermi* Science Tools version `v9r33p0-fssc-20140520`.

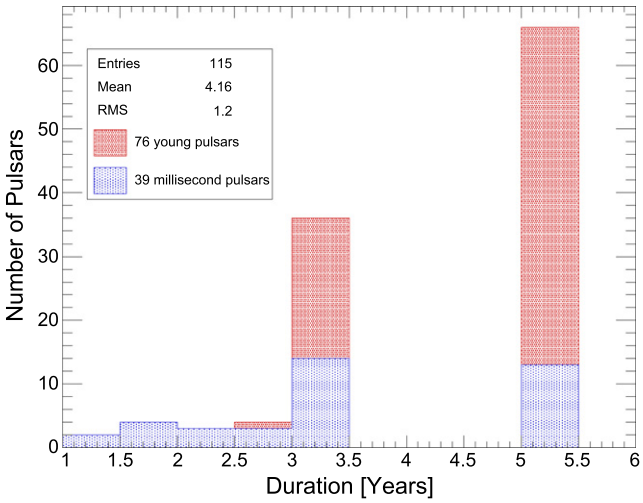

Figure 1. Histogram of the duration of the individual pulsar data sets used in this analysis. The duration is entirely determined by the period of validity of the available pulsar timing solutions.

3. AP PULSAR ANALYSIS

Spectral analysis of *Fermi*-LAT data is typically performed through a maximum likelihood fitting procedure where the photon event data are fit to a positional and spectral model. The flux for a particular source is then derived from the best fit model. The *Fermi*-LAT data can also be analyzed with an AP method where the raw event counts from a particular region of interest (ROI) on the sky are combined with a measure of the instrument exposure (cm^2 s) to the region to determine the flux. The online *Fermi*-LAT analysis manual reports that the AP method is less accurate and less sensitive than the likelihood fitting procedure but that it "provides a model independent measure of the flux" and it "is less computationally demanding."[4] We demonstrate here that the AP method can be used to produce accurate SEDs for pulsars from multi-year data sets. This type of analysis is possible due to the accurate determination of the background rate which can be measured in the *Off* phase range.

3.1. AP Analysis Steps

The processing follows closely the AP analysis thread detailed in the online *Fermi*-LAT analysis manual.[4]

1. Logarithmically spaced energy binning with 4 bins per decade is chosen over the 100 MeV–1 TeV energy range.
2. An ROI is chosen around each pulsar with an energy-dependent radius. The radius chosen is three times the 68% point-spread function (PSF) containment radius determined from a Vela analysis by Ackermann et al. (2013a) which ranges from 2.°26 at 100 MeV to 0.°15 at 10 GeV.[5] In order to maintain sufficient statistics at high

[3] www.slac.stanford.edu/~kerrm/fermi_pulsar_timing/

[4] http://fermi.gsfc.nasa.gov/ssc/data/analysis/scitools/aperture_photometry.html

[5] The size of the *Fermi*-LAT PSF depends on which region of the instrument the pair conversion occurs in. In this analysis the size of the ROI was tied to the size of the "Front" PSF.

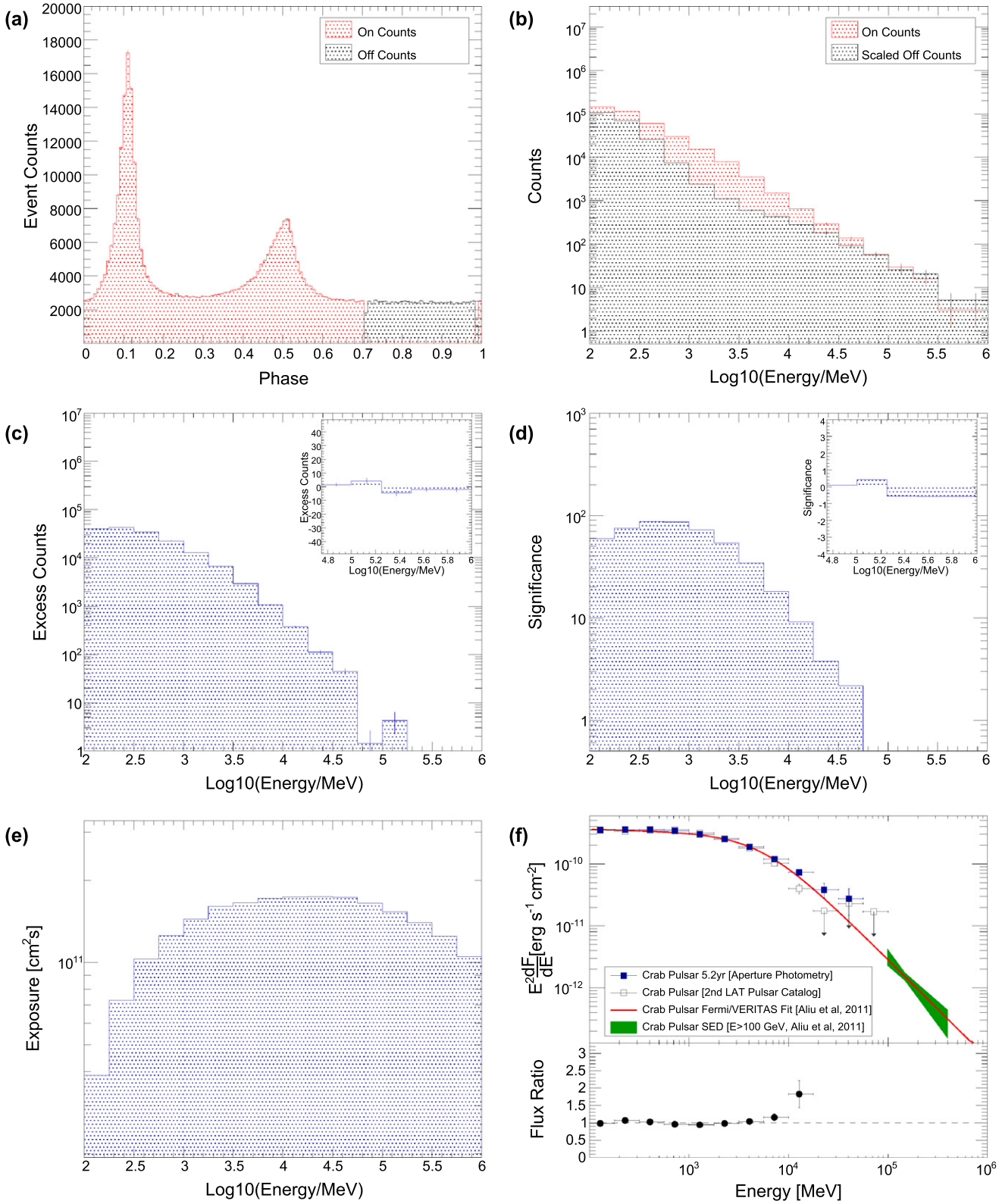

Figure 2. Aperture photometry analysis steps for the Crab pulsar. Panel (a) plots the phase distribution (light curve) of the Crab pulsar from 5.2 yr of *Fermi*-LAT observations. The *Off* phase range, [0.71–0.99], is defined in the second *Fermi*-LAT catalog of gamma-ray pulsars (2PC). Panel (b) plots the distribution of photon energies for events which fell in the *On* and *Off* phase ranges. The *Off* events have been scaled by α which is the ratio of the *On* phase gate(s) size to the *Off* gate(s) size. Panel (c) shows the energy distribution of the excess events and panel (d) shows the significance of the excess in each energy bin. Panel (e) shows the *Fermi*-LAT exposure for the ROI used in each energy bin determined from `gtexposure`. In panel (f) the Crab pulsar AP SED is plotted alongside the Crab pulsar SED determined from a likelihood fit done in the 2PC. A broken power-law fit to *Fermi*-LAT and VERITAS data from Aliu et al. (2011) is plotted, as well as the VERITAS >100 GeV bow-tie. Below the SED plotted in panel (f) is the ratio of the AP flux to the 2PC flux in each bin, showing the level of agreement between the AP method and the likelihood method.

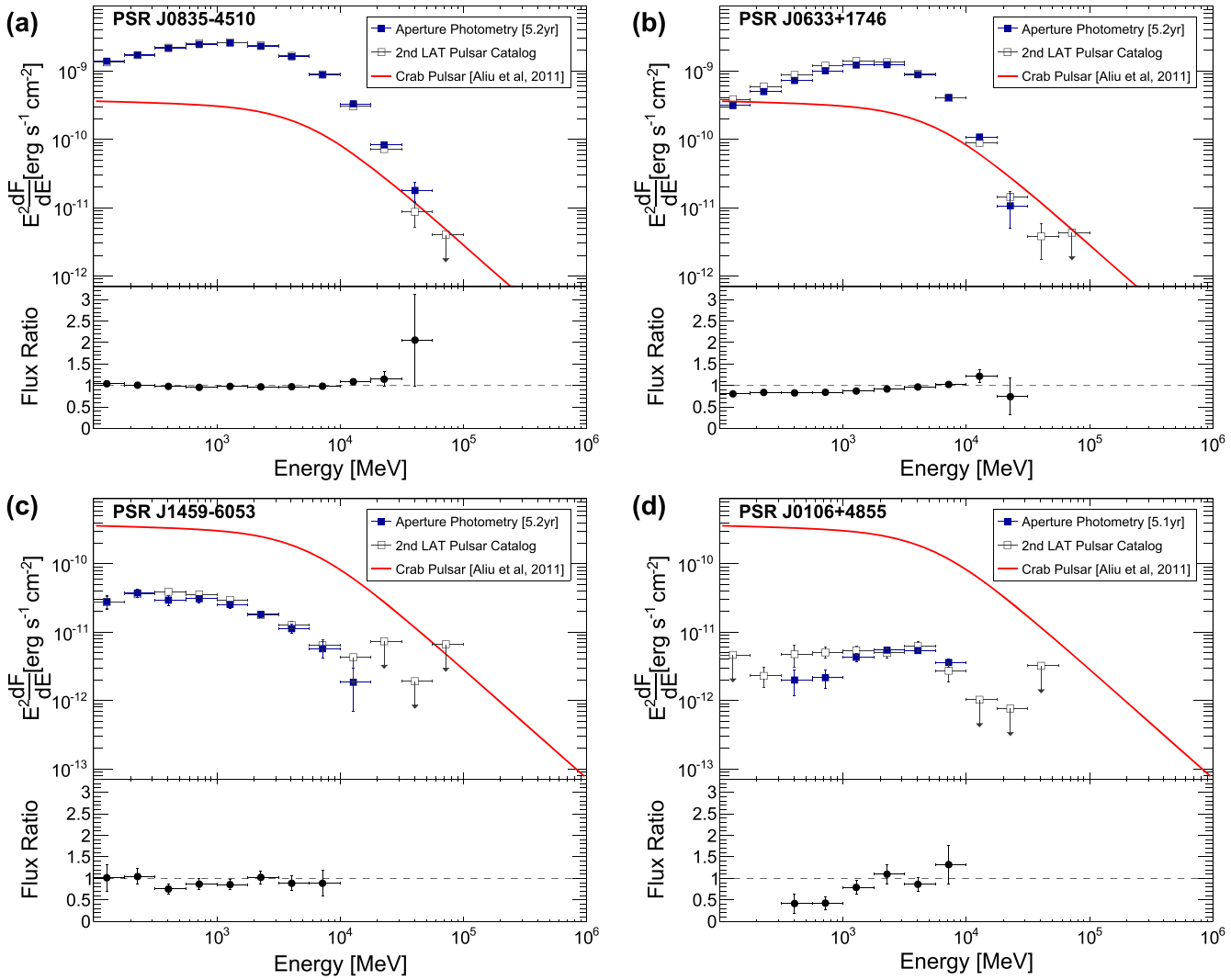

Figure 3. Example SEDs determined with the AP method. The well known Vela and Geminga pulsars are shown in panels (a) and (b), respectively, with two newly discovered dimmer gamma-ray pulsars shown in panels (c) and (d). In each panel the AP SED is plotted alongside the SED determined from a likelihood fit done in the 2PC. A broken power-law fit to the Crab pulsar data from Aliu et al. (2011) is plotted for scale. Below each SED plot, the ratio of the AP flux to the 2PC flux is plotted for bins where a $>1.5\sigma$ excess is derived in the AP analysis and a flux value is reported by the 2PC.

energies, the radius of the ROI was fixed to $3 \times 0.^{\circ}15$ above 10 GeV.

3. The *Fermi*-LAT analysis tools `gtselect`, `gtmktime`, `gtbin`, and `gtexposure` are then run over each pulsar with the corresponding radial and energy selections for all observations performed within the period of validity of the pulsar timing solution.
4. The photon event list is then barycentered and phase-folded using the `Tempo2` package (Hobbs et al. 2006) with the *Fermi* `Tempo2` plugin and the corresponding timing solution.
5. For the 66 pulsars where timing solutions other than those provided by the 2PC were used, a cross-correlation analysis was performed on the phase data to determine the phase offset between the derived pulsar light curve and the light curve published in the 2PC supplementary material. The phase data is then corrected for this phase offset to ensure that the (arbitrary) 2PC definition of phase zero is maintained in this analysis so that the defined *Off* phase region remains valid.
6. Within each energy bin, a cut on phase is applied and events which fall within the *Off* phase region and those which fall outside this region—the *On* phase region—are selected. The ratio of the size of the *On* phase range to the size of the *Off* phase range, defined as α, is then used to scale the number of event counts in the *Off* phase region ($N_{\rm off}$) to the number in the *On* region ($N_{\rm on}$).
7. The number of excess pulsed events is then defined as $N_{\rm ex} = N_{\rm on} - \alpha N_{\rm off}$ and the flux is $N_{\rm ex}$ divided by the exposure ($\mathcal{T}$) calculated in step 3 using `gtexposure`. The significance of the excess is calculated using Equation (17) from Li & Ma (1983).

Following this procedure we derive the energy distributions for the *On* and *Off* phase regions, and the instrument exposure, for all 115 pulsars under study. These distributions, along with the derived AP SED, are shown for the Crab pulsar in Figure 2. The SEDs for several other pulsars derived using the AP method are plotted in Figure 3. Using the AP method, 19 pulsars are detected above 10 GeV and all, bar one, appear in the *Fermi*-LAT catalog of sources above 10 GeV (Ackermann

Table 1
Properties of 19 Pulsars Detected in the 10–17 GeV Energy Bin with the AP Method whose Excess Exceed 3σ

Name	Excess	Flux ($\times 10^{-10}$cm^{-2}s^{-1})	Significance σ
PSR J0007+7303	289.7 ± 18.9	11.6 ± 0.8	15.4
PSR J0534+2200	377.3 ± 41.4	21.7 ± 2.4	9.1
PSR J0633+0632	11.4 ± 3.4	0.7 ± 0.2	3.4
PSR J0633+1746	542 ± 52.6	32.0 ± 3.1	10.3
PSR J0835−4510	1703 ± 60.4	98.1 ± 3.5	28.2
PSR J1028−5819	81.8 ± 12.1	4.3 ± 0.6	6.7
PSR J1048−5832	32 ± 9.4	1.7 ± 0.5	3.4
PSR J1413−6205	46.7 ± 12.3	2.4 ± 0.6	3.8
PSR J1420−6048	44.3 ± 13.6	2.3 ± 0.7	3.2
PSR J1620−4927	43.5 ± 13.5	2.5 ± 0.8	3.2
PSR J1709−4429	373 ± 22.4	21.5 ± 1.3	16.6
PSR J1732−3131	47.3 ± 11.8	2.8 ± 0.7	4.0
PSR J1809−2332	96.3 ± 12.5	5.9 ± 0.8	7.7
PSR J1907+0602	47.1 ± 9.9	2.9 ± 0.6	4.8
PSR J2017+0603	18.1 ± 3.9	1.1 ± 0.2	4.6
PSR J2021+3651	86.8 ± 14.9	4.7 ± 0.8	5.8
PSR J2032+4127	43.2 ± 7.5	2.3 ± 0.4	5.8
PSR J2111+4606	23.8 ± 5.3	1.2 ± 0.3	4.5
PSR J2229+6114	53.6 ± 9.4	2.3 ± 0.4	5.7

Note. The Crab pulsar is excluded from the stacking analysis but is included here for completeness. The excesses, fluxes, and significances are quoted for the 10–17 GeV energy range only. All entries, bar PSR J1732-3131, are also listed in the 1FHL catalog. PSR J2017+0603 is the only millisecond pulsar in the list.

et al. 2013b). The properties of these 19 pulsars are listed in Table 1.

3.2. Performance of the AP Method

Assuming that the 2PC flux values are indeed more accurately measured than the AP flux, we can examine the ratio of the AP flux to the 2PC flux to assess the performance of the AP method. This ratio is plotted for individual pulsars below the SED panels in Figures 2 and 3. Profile histograms of this ratio for 83 of the pulsars under study as shown in Figure 4. 33 pulsars are excluded from these profiles and account for cases where no SED is derived in the 2PC (10), where no $>1.5\sigma$ excess are derived in the AP analysis (3), or where the pulsar is so weak in the 2PC analysis that a 2 bins per decade binning is chosen instead of the usual 4 (20).

Examining Figure 4(a) we see that on average, the AP flux is ∼10% lower than the 2PC flux, although there are trends affecting the ratio in different energy ranges. Above 10 GeV the AP flux is, on average, overestimated by ∼15–20%. There is also a sizable scatter, particularly at low energies ($E < 500$ MeV) where the rms of the flux ratio can be as large as 60%. It is important to point out that this AP framework does not measure the total flux from a pulsar, but the difference in the flux level between the *On* and *Off* phase regions. In contrast, the likelihood fitting employed in the *Fermi*-LAT analysis measures the total flux over all phases, except in (8) cases like the Crab pulsar where the *Off* phase region is used to model un-pulsed nebular-like emission which is then subtracted from the total. Given that this AP method does not measure the total flux over all phases, it is not surprising that it returns a lower flux than the 2PC, on average. Figure 4(b) shows that above 5 GeV the average flux ratio is ∼1 with only a weak dependence on the flux value, although at low fluxes ($\mathrm{Flux}_{2\mathrm{PC}} < 3 \times 10^{-12}$ ergs s^{-1} cm^{-2}) the AP flux is, on average, 20% higher with a 30% scatter. Given this behavior of the flux ratio at high energies and low fluxes, we estimate a systematic uncertainty at the level of 60% on the stacked flux values and limits presented above 30 GeV in Section 4.

We wish to point out that these systematic uncertainties do not effect our ability to detect emission, only our ability to derive the corresponding flux level or flux limit. Since the SED is expected to fall exponentially above the GeV break in curvature radiation models, any significant stacked detection above ∼100 GeV would lie in strong tension with exponential cut-off predictions, regardless of the uncertainty on the corresponding flux level.

3.3. Stacking Analysis

Knowing the α values, and having calculated the distribution of N_{on}, N_{off}, and $\mathcal{T}$ versus energy for each pulsar, it is quite

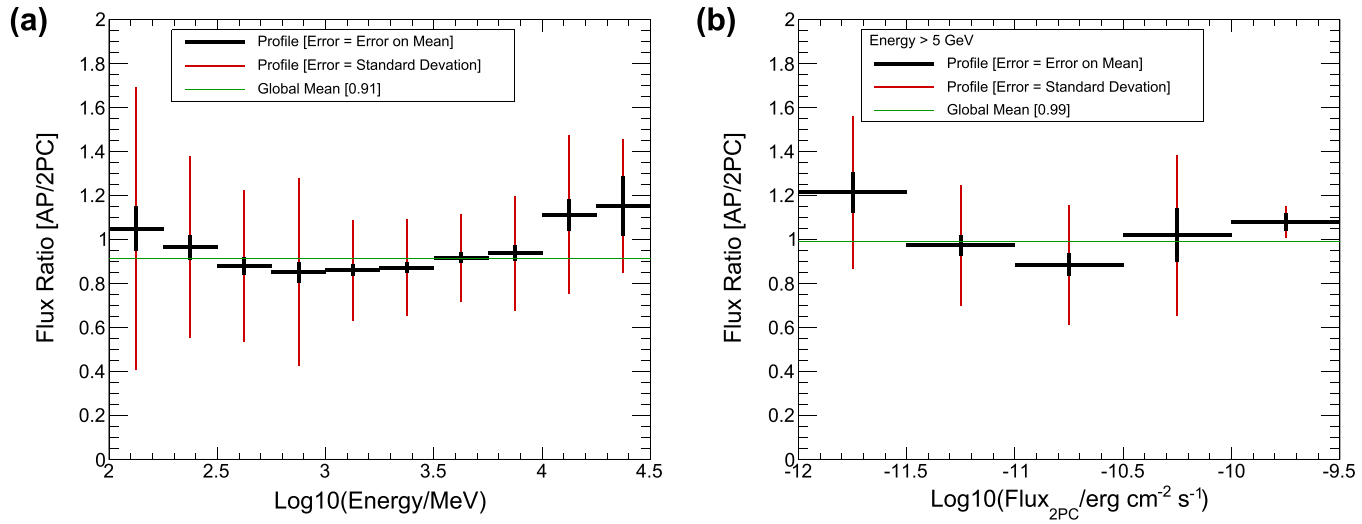

Figure 4. Ratio of the AP flux to the 2PC flux plotted in profile histograms for 83 of the pulsars under study. In panel (a) the ratio is plotted against the bin energy while in panel (b) the ratio is plotted against the measured 2PC flux for bin energies above 5 GeV.

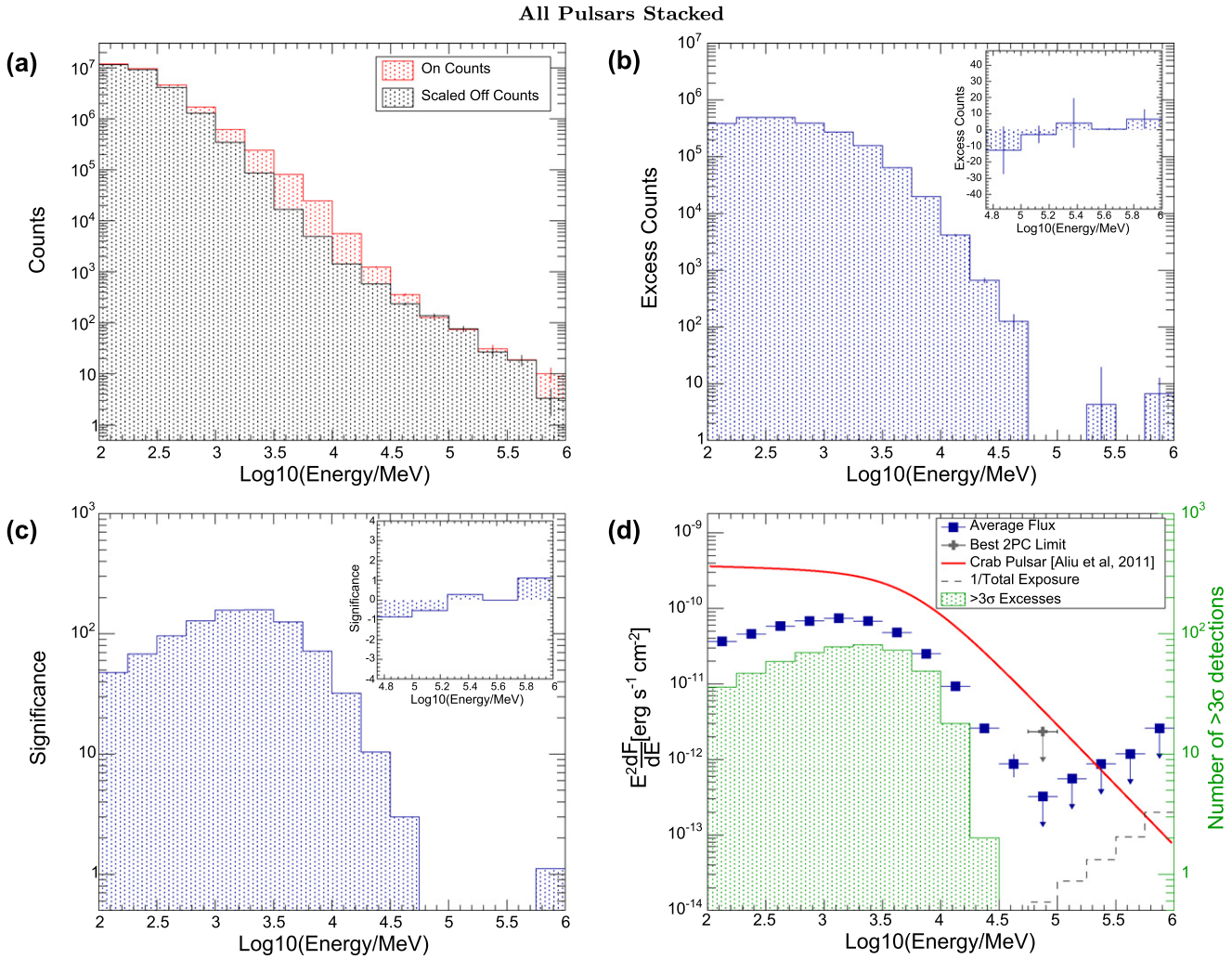

Figure 5. Stacked analysis for all 115 pulsars under study. Panel (a) shows the energy distribution of the total event counts from all *On* phase regions alongside the total α-scaled event counts from all *Off* phase regions. Panels (b) and (c) show the corresponding excesses and significances, respectively. The inserts in these panels show the same distributions with a zoom-in on the bins above ~50 GeV and with a linear scale on the y-axis. Panel (d) shows the average flux (square markers) determined by dividing the total excess by the total exposure (see Section 3.3). The dashed-line histogram shows one over the total exposure, indicating the flux which would correspond to a single excess photon. This is the minimum possible flux which could be measured given the total exposure. The gray cross shows the most constraining limit on emission from a single pulsar in the 56.2–100 GeV range presented in the 2PC. The 2PC presented no limits at higher energies. The broken power-law fit to the Crab pulsar data from Aliu et al. (2011) is plotted for scale. The dot-filled histogram (y-axis scale is on the right) indicates how many individual pulsars showed excesses which measured above 3σ in each energy range. 18 were detected in the 10–17 GeV energy bin and they a listed in Table 1.

simple to determine the total excess,

$$\mathrm{Ex}^{b}_{\mathrm{tot}} = \sum_{i=1}^{N}\left(N^{i,b}_{\mathrm{on}} - \alpha^{i} N^{i,b}_{\mathrm{off}}\right), \tag{1}$$

the total exposure,

$$\mathcal{T}^{b}_{\mathrm{tot}} = \sum_{i=1}^{N} \mathcal{T}^{i,b}, \tag{2}$$

and thus, the average flux,

$$\mathrm{Flux}^{b}_{\mathrm{av}} = \frac{\mathrm{Ex}^{b}_{\mathrm{tot}}}{\mathcal{T}^{b}_{\mathrm{tot}}}, \tag{3}$$

for N pulsars in a given energy bin, b. The corresponding significance of the total excess is determined by the generalized version of Equation (17) from Li & Ma (1983; see Aharonian et al. 2004), which accepts subsets of data with different α values. For cases where the significance of the total excess is less than 2σ, the method of Helene (1983) is used to derive the 95% confidence-level upper limit on the total excess, which is in turn divided by the total exposure to determine the corresponding flux upper limit. These procedures are used to derive the results presented in the following section.

4. RESULTS

The results of the stacking analysis for the entire pulsar sample are presented in Figure 5. The stacking analysis results for the separate young pulsar and millisecond pulsar ensembles are shown in Figures 6 and 7, respectively. No significant excesses are seen in any of these analyses at energies above 50 GeV. Upper limits on the average flux, determined at the 95% confidence-level, are listed in Table 3 for three energy bins above 50 GeV. Limits are also presented in units of the Crab pulsar where the broken power-law fit to the *Fermi*-LAT

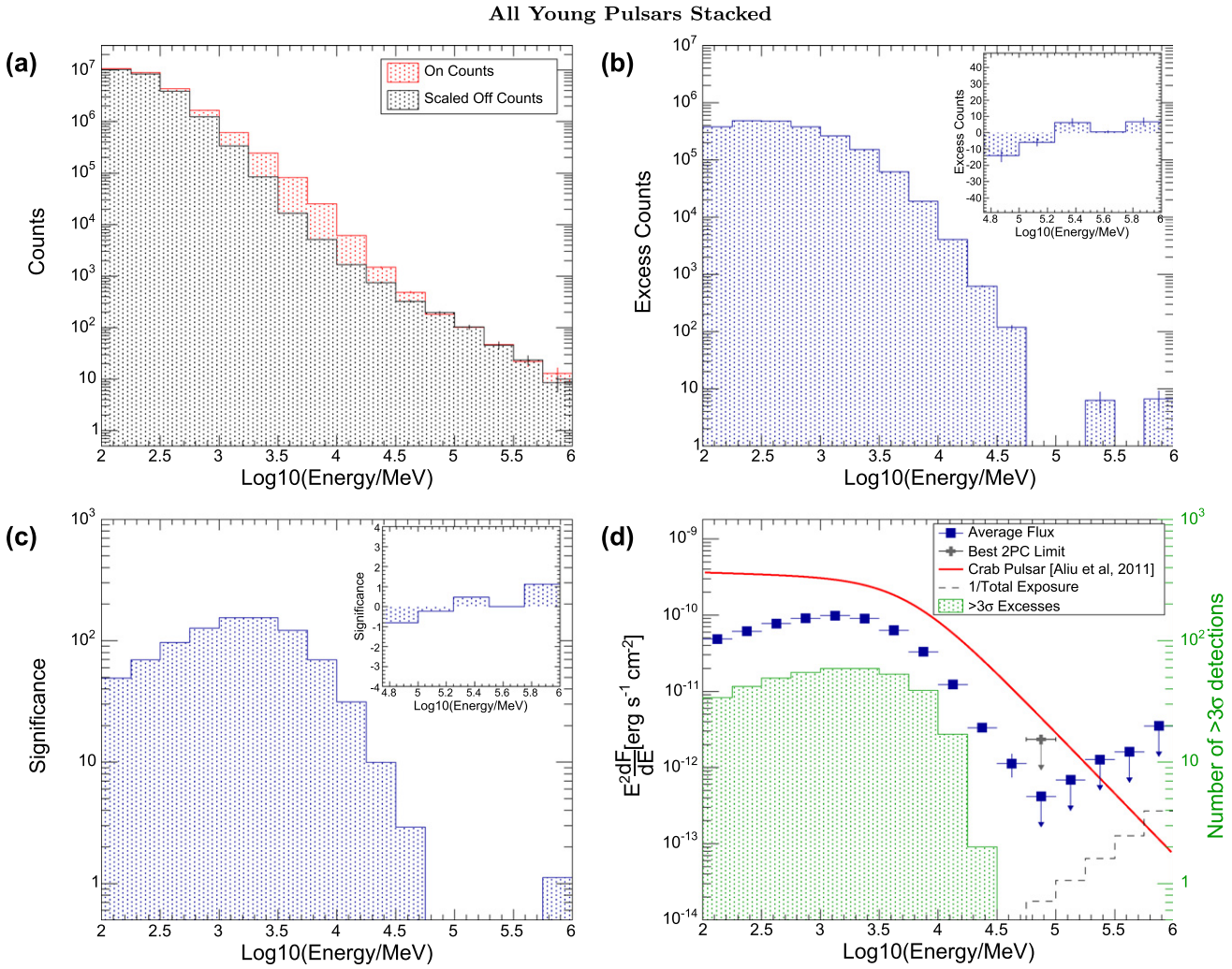

Figure 6. Stacked analysis for all of the 76 young pulsars under study. See the caption of Figure 5 for a full description of each panel.

and VERITAS data presented in Aliu et al. (2011) defines a Crab pulsar unit.

In addition to these analyses, we stacked sub-samples of the data where each sub-sample was composed of the 10 pulsars with the largest value of a given parameter. Sub-sample selections based on gamma-ray luminosity (L_γ), spin-down power ($\dot{E}$), spin-down power over distance squared ($\dot{E}/d^2$), gamma-ray photon flux (F_{100}), and non-thermal X-ray energy flux ($F_X^{\rm nt}$) were investigated and are listed in Table 2.[6] No significant excesses were observed above 50 GeV in any of these sub-sample stacking analyses.

The shape of the average young pulsar and average millisecond pulsar SEDs were categorized by fitting a power law times a super-exponential cut-off function

$$E^2\frac{dF}{dE} = A\left(\frac{E}{1\ \mathrm{GeV}}\right)^{\Gamma} e^{-\left(\frac{E}{E_{\rm cut}}\right)^b} \quad (4)$$

to the SED data. These fits are presented in Figure 8. Fixing $b = 1$ reduces Equation (4) to a power law times an exponential cut-off function and, as expected, this functional form does not reproduce the sub-exponential fall of the SED above the break. However, it can be used to measure the average flux-weighted value of the spectral index (Γ) and cut-off ($E_{\rm cut}$) parameters (Abdo et al. 2013). It is clear from Figure 8 that the average SEDs have qualitatively the same shape, with the average flux from the 39 millisecond pulsars about an order of magnitude lower than the average flux from the 76 young pulsars. The spectral parameters derived from the fitting are remarkably similar. The best fit Γ value is 0.54 ± 0.05 for the millisecond pulsars and 0.41 ± 0.01 for the young pulsars, while the best fit $E_{\rm cut}$ values are 3.60 ± 0.21 GeV and 3.54 ± 0.04 GeV, respectively. Allowing b to float we find that sub-exponential forms ($b < 1$) are preferred, with the best-fit b value of 0.59 ± 0.02 for the young pulsars and 0.7 ± 0.15 for the millisecond pulsars. Note that only statistical uncertainties on the SED data points were used during the fitting and thus the uncertainty on the best-fit parameter values are likely underestimated.

5. DISCUSSION AND CONCLUSION

Following a stacked analysis of 115 gamma-ray pulsars, with an average exposure of ~4.2 yr per pulsar, we find no evidence of cumulative emission above 50 GeV. Stacked searches exclusive to the young pulsars, the millisecond pulsars, and

[6] The Crab pulsar was excluded from all of these sub-sample stacking analyses. The parameter values listed in the 2PC catalog were used in all cases.

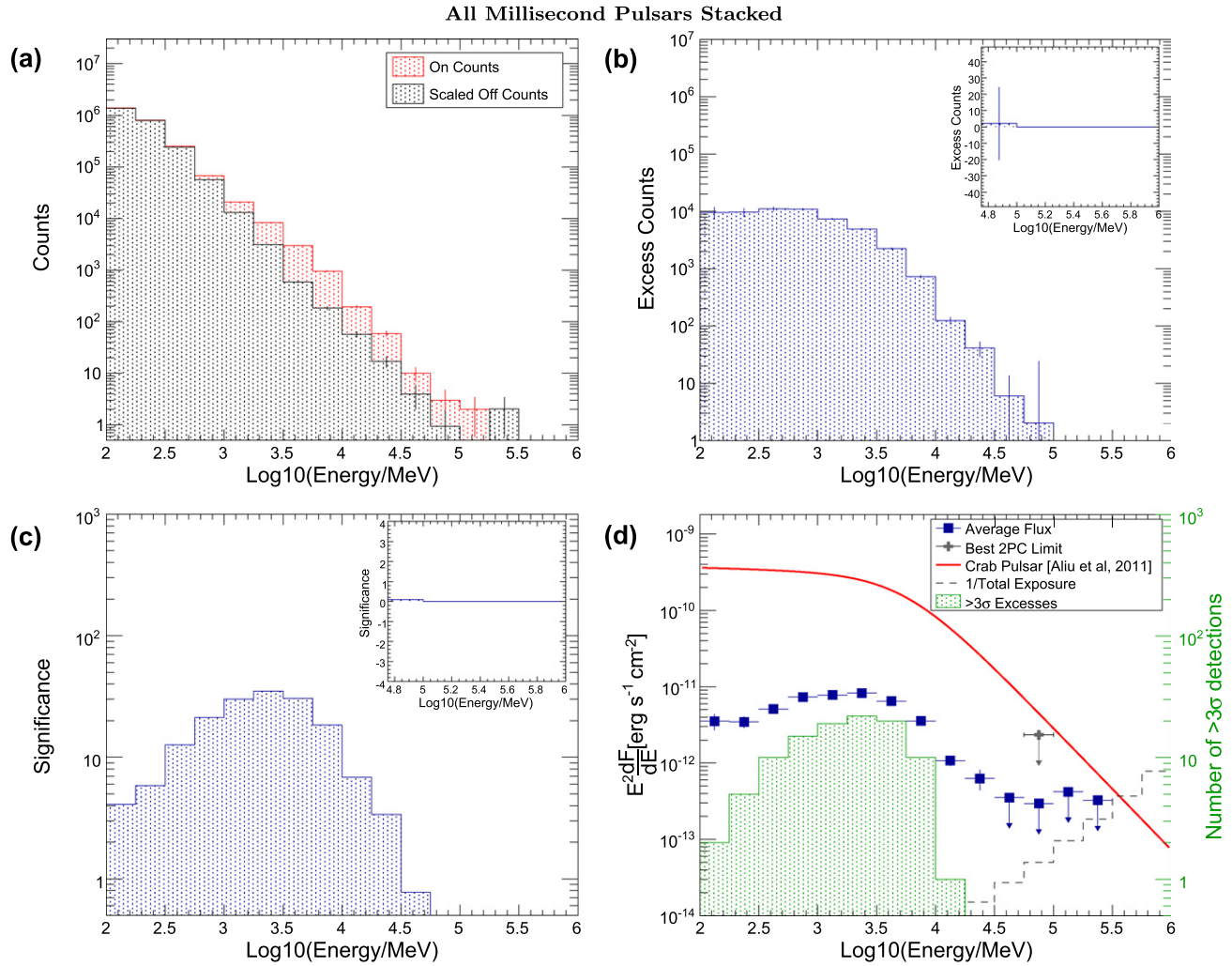

Figure 7. Stacked analysis for all 39 millisecond pulsars under study. See the caption of Figure 5 for a full description of each panel. PSR J2017+0603 is the only millisecond pulsar with a >3σ excess measured in the 10–17 GeV energy bin (see Table 1 for a description of this excess).

several other promising sub-samples also return no significant excesses above 50 GeV. Any average emission present in the entire pulsar sample is limited to be below ~7% of the Crab pulsar in the 56–100 GeV band and to be below ~30% in the 100–177 GeV band. The average flux limits presented in Table 3 are roughly three times lower than the best flux limits achieved in dedicated individual pulsar analyses done in the 2PC in the 56–100 GeV band.

One should note that a limit on the average flux from 115 pulsars at 7% of the Crab pulsar level is consistent with, for example, a scenario in which all 115 pulsars emit at 7% of the Crab pulsar level. It is also consistent with a scenario in which eight pulsars emit at 100% the level of the Crab pulsar and the remaining 107 pulsars have zero emission. Therefore this analysis does not exclude the possibility of finding several pulsars that are as bright as the Crab pulsar above 50 GeV, or several dozen which are ten times dimmer.[7] It does, however, constrain the average flux from the ensemble, and therefore, for every individual pulsar detected above this flux limit, the average emission from the remaining pulsars is constrained to be further below the limit.

In the 100 MeV to ~50 GeV energy range we find that the average SEDs returned from the young pulsar and millisecond pulsar stacking analyses are very similar in shape and are generally compatible with a power law times a sub-exponential cut-off. Abdo et al. (2010) and Celik & Johnson (2011) have shown that a sub-exponential cut-off function approximates a superposition of exponential cut offs, thus the appearance of a sub-exponential cut-off in the ensemble SED is to be expected within a curvature radiation model. We note, however, that the highest energy spectral point is higher than the best fit sub-exponential cut-off function at the ~2.4σ level in both the young pulsar and millisecond pulsar cases. This cannot be taken as strong evidence for a non-exponentially suppressed pulsar emission component aggregating in the stacked analysis, however, the available data cannot rule it out beyond the level of the limits shown in Figures 5–7 and Table 3.

At energies above 100 GeV, individual pulsar limits made by air Cherenkov telescopes are much stronger than those achievable with the *Fermi*-LAT. For example, the sensitivity necessary to detect the Crab pulsar emission above 100 GeV at the ~5σ level is achieved by VERITAS in under 30 hr. Beyond this work, improvements can be made using the forthcoming

[7] This point is illustrated by the fact that the Vela pulsar has recently been shown to emit at ~130% of the Crab pulsar level in the 50–100 GeV energy range (Leung et al. 2014).

Table 2
The List of the Pulsars used in the Sub-sample Stacking, where the • Symbol Denotes the Inclusion of the Pulsar in the given Sample

Name	L_γ	$\dot{E}$	$\dot{E}/d^2$	F_{100}	$F_X^{\rm nt}$
PSR J0205+6449	⋯	•	•	⋯	•
PSR J0437−4715	⋯	⋯	⋯	⋯	•
PSR J0633+1746	⋯	⋯	•	•	⋯
PSR J0835−4510	⋯	•	•	•	•
PSR J1023−5746	⋯	•	⋯	⋯	⋯
PSR J1048−5832	•	⋯	⋯	⋯	⋯
PSR J1112−6103	•	⋯	⋯	⋯	⋯
PSR J1119−6127	•	⋯	⋯	⋯	⋯
PSR J1124−5916	⋯	•	•	⋯	•
PSR J1410−6132	•	•	⋯	⋯	⋯
PSR J1418−6058	⋯	⋯	•	•	⋯
PSR J1420−6048	•	•	⋯	⋯	⋯
PSR J1513−5908	⋯	•	•	⋯	•
PSR J1709−4429	•	⋯	•	•	⋯
PSR J1747−2958	•	⋯	⋯	⋯	•
PSR J1801−2451	⋯	⋯	⋯	⋯	•
PSR J1809−2332	⋯	⋯	⋯	•	⋯
PSR J1813−1246	⋯	•	⋯	•	⋯
PSR J1826−1256	⋯	⋯	⋯	•	⋯
PSR J1833−1034	⋯	•	•	⋯	•
PSR J1836+5925	⋯	⋯	⋯	•	⋯
PSR J1907+0602	•	⋯	⋯	⋯	⋯
PSR J1952+3252	⋯	⋯	•	⋯	•
PSR J2021+3651	•	⋯	⋯	•	⋯
PSR J2021+4026	•	⋯	⋯	•	⋯
PSR J2229+6114	⋯	•	•	⋯	•

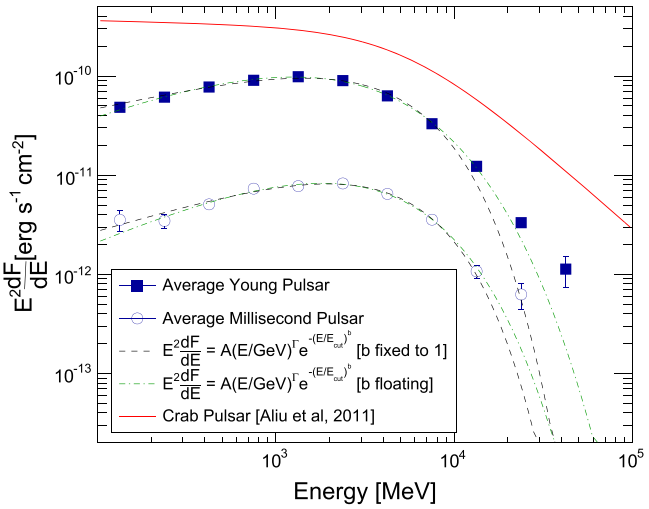

Figure 8. Average SEDs derived from the stacking of the 76 young pulsars and 39 millisecond and pulsars. The SEDs are each fit with a power law times a super-exponential cut-off keeping b both fixed to unity and allowing it to float. For the pure exponential cut-off case ($b = 1$) the best-fit Γ value is 0.54 ± 0.05 for the millisecond pulsars and 0.41 ± 0.01 for the young pulsars while the best fit $E_{\rm cut}$ values are 3.60 ± 0.21 GeV and 3.54 ± 0.04 GeV, respectively. Allowing b to float we find that sub-exponential forms ($b < 1$) are preferred, with the best-fit b value of 0.59 ± 0.02 for the young pulsars and 0.7 ± 0.15 for the millisecond pulsars. The broken power-law fit to the Crab pulsar data from Aliu et al. (2011) is plotted for scale.

Table 3
Limits at the 95% Confidence Level on the Average Flux from Stacked Ensembles of Gamma-ray Pulsars

	All		Young Pulsars		Millisecond Pulsars	
Energy Range (GeV)	Flux Limit ($\times 10^{-12}$ cm^{-2} s^{-1})	Flux Limit (Crab pulsar units)	Flux Limit ($\times 10^{-12}$ cm^{-2} s^{-1})	Flux Limit (Crab pulsar units)	Flux Limit ($\times 10^{-12}$ cm^{-2} s^{-1})	Flux Limit (Crab pulsar units)
56.2–100	1.57	0.07	2.03	0.09	1.44	0.07
100–177	1.52	0.31	1.88	0.38	1.14	0.23
177–316	1.34	1.21	1.96	1.76	0.50	0.45

Note. The limit values presented in Crab pulsar units assume the broken power-law fit to the Crab pulsar data from Aliu et al. (2011) is a Crab pulsar flux unit.

Fermi-LAT Pass-8 data release which will improve the *Fermi*-LAT acceptance by ∼25% at 100 GeV (Atwood et al. 2013). Improvements to this stacking analysis can also be made by employing a likelihood framework to stack the sources (see Ackermann et al. 2011 for an example), rather than the simple *On* minus *Off* procedure described here. The flux sensitivity of any stacking analysis will, however, ultimately be bounded by the exposure of the *Fermi*-LAT. The dashed-line histograms (one over the total exposure) in Figures 5–7 indicate that limits derived in this analysis are factors of ∼4–20 times larger than the minimum measurable average flux in the 100–177 GeV range. A future stacking analysis which doubles both the number of pulsars and the duration of observation used will increase the exposure term by factor of a four indicating that future stacking analyses that do not yield detections may improve on the limits presented here by perhaps one or two orders of magnitude.

The author is supported in part by the Kavli Institute for Cosmological Physics at the University of Chicago through grant No. NSF PHY-1125897 and an endowment from the Kavli Foundation and its founder Fred Kavli. I am grateful to Pat Moriarty, David Hanna, Nepomuk Otte, and Benjamin Zitzer for their comments on the early drafts of this manuscript. I appreciate the anonymous referee for the comments and suggestions made during the review process.

REFERENCES

Abazajian, K. N., & Kaplinghat, M. 2012, PhRvD, 86, 083511
Abdo, A. A., Ackermann, M., Ajello, M., et al. 2010, ApJ, 713, 154
Abdo, A. A., Ajello, M., Allafort, A., et al. 2013, ApJS, 208, 17
Ackermann, M., Ajello, M., Albert, A., et al. 2011, PhRvL, 107, 241302
Ackermann, M., Ajello, M., Allafort, A., et al. 2013a, ApJ, 765, 54
Ackermann, M., Ajello, M., Allafort, A., et al. 2013b, ApJS, 209, 34
Aharonian, F., Akhperjanian, A., Beilicke, M., et al. 2004, A&A, 421, 529
Aharonian, F. A., Bogovalov, S. V., & Khangulyan, D. 2012, Natur, 482, 507

Aleksić, J., Alvarez, E. A., Antonelli, L. A., et al. 2011, ApJ, 742, 43
Aleksić, J., Alvarez, E. A., Antonelli, L. A., et al. 2012, A&A, 540, A69
Aliu, E., Arlen, T., Aune, T., et al. (The VERITAS Collaboration) 2011, Sci, 334, 69
Aliu, E., Archambault, S., Archer, A., et al. 2015, ApJ, 800, 61
Atwood, W., Albert, A., Baldini, L., et al. 2013, arXiv:1303.3514
Celik, O., & Johnson, T. J. 2011, in AIP Conf. Proc. 1357, Radio Pulsars: An Astrophysical Key to Unlock the Secrets of the Universe, ed. M. Burgay et al. (Melville, NY: AIP), 225
Cheng, K. S., Ho, C., & Ruderman, M. 1986, ApJ, 300, 522
Du, Y. J., Qiao, G. J., & Wang, W. 2012, ApJ, 748, 84
Harding, A. K., Stern, J. V., Dyks, J., & Frackowiak, M. 2008, ApJ, 680, 1378
Helene, O. 1983, NIMPR, 212, 319
Hirotani, K. 2001, ApJ, 549, 495
Hobbs, G. B., Edwards, R. T., & Manchester, R. N. 2006, MNRAS, 369, 655
Jackson, B., Scargle, J. D., Barnes, D., et al. 2005, ISPL, 12, 105
Leung, G. C. K., Takata, J., Ng, C. W., et al. 2014, ApJL, 797, LL13
Li, T.-P., & Ma, Y.-Q. 1983, ApJ, 272, 317
Lyutikov, M., Otte, N., & McCann, A. 2012, ApJ, 754, 33
Lyutikov, M. 2012, ApJ, 757, 88
Lyutikov, M. 2013, MNRAS, 431, 2580
Pétri, J. 2012, MNRAS, 424, 2023
Romani, R. W. 1996, ApJ, 470, 469
Story, S. A., & Baring, M. G. 2014, ApJ, 790, 61
Scargle, J. D., Norris, J. P., Jackson, B., & Chiang, J. 2013, ApJ, 764, 167
Takata, J., & Chang, H.-K. 2007, ApJ, 670, 677